Research Square

Preprints are preliminary reports that have not undergone peer review.
They should not be considered conclusive, used to inform clinical practice,
or referenced by the media as validated information.

Migration of aerobic bacteria from the duodenum to the pancreas with tumors: a mechanistic understanding

Hiroaki Shirai (hs7796@keio.jp)
Keio University
Cocoro Ito
Keio University
Kosuke Tsukada
Keio University

Research Article

Keywords: pH taxis, microfluidics, mathematical modeling, pancreatic cancer, microbiome

Posted Date: October 1st, 2021

DOI: https://doi.org/10.21203/rs.3.rs-948107/v1

License: This work is licensed under a Creative Commons Attribution 4.0 International License.
Read Full License

Migration of aerobic bacteria from the duodenum to the pancreas with tumors: a mechanistic understanding

.

Hiroaki Shirai[a*] Cocoro Ito[b], Kosuke Tsukada[a,b]

[a]Graduates School of Science and Technology, Keio University, 3-14-1 Hiyoshi Kohoku-ku, Yokohama-shi, Kanagawa, Japan 223-8522

[b]Faculty of Science and Technology, Keio University

Hiroaki Shirai.

Email: hs7796@keio.jp

Author Contributions: Hiroaki Shirai performed the entire work, wrote the manuscript, performed microfluidic experiments, and performed mathematical modeling. Cocoro Ito designed and fabricated the microfluidic device. Kosuke Tsukada is PI of the laboratory, obtained funding, provided research equipment, and managed the laboratory.

Keywords: pH taxis, microfluidics, mathematical modeling, pancreatic cancer, microbiome.

Abstract

More aerobic bacteria are found in the pancreas with tumors than in the healthy pancreas. We provide a mechanistic understanding of the migration of intestinal bacteria from the duodenum to the pancreas with tumors. Mathematical models of migration of aerobic bacteria from the duodenum to the pancreas with tumors in the hepatopancreatic duct were developed. In addition, the behaviors of GFP *E. coli* under a pH gradient in a microfluidic device were analyzed. Moreover, upstream migrations of *Pseudomonas fluorescens* against flow were measured in a

polydimethylsiloxane (PDMS) T-shaped cylinder mimicking a pancreatic duct. The simulated bacterial concentration of the pancreas with tumors was higher than that of the healthy pancreas and agreed reasonably well with the literature. Migration of aerobic bacteria in the hepatopancreatic duct is counteracted by bile and pancreatic juice flow but facilitated greatly by bacterial pH taxis from lower pH in duodenum fluid toward slightly alkaline pH in pancreatic juice, favorable for them. Migration of bacteria to the pancreas with tumors is made easier by solid tumors on the pancreatic duct, which compresses the pancreatic duct and thus reduces the fluid flow rate. On the other hand, GFP *E. coli* migrated under the pH gradient in a microfluidic device from acidic areas toward neutral or slightly alkaline pH, validating pH taxis. Furthermore, *Pseudomonas fluorescens* migrated upstream from hydrochloride solution but not from bicarbonate solution against bicarbonate flow at >20 μm/s, with an advancing velocity of approximately 60 μm/s, validating the models (244 words).

Main Text

1. Introduction

Effective treatment against pancreatic cancer with a five-year survival rate of 5–10% is urgent (1). The interactions between cancer and bacteria have widely been accepted, such as the roles of gut microbes in immunotherapy(2). The pancreas, adjacent to and connected via the pancreatic duct to the duodenum, a part of the small intestine with abundant intestinal bacteria, provides a unique niche for cancer researchers (3–14), including a link between the oral microbiome and risk of pancreatic cancer(3), bacteria found in pancreatic cystic fluid (4), bacterial infection in the pancreas with pancreatitis and its association with cancer risk (5, 6), roles in carcinogenesis (7, 8), and bacteria in tumors affecting cancer treatment (9–14). For example, human pancreatic ductal adenocarcinomas (PDACs) contain aerobic bacteria at higher levels than healthy pancreases (10, 12) (Table S1), commonly favoring neutral pH, such as *Pseudomonas*(15), *Citrobacter*(16), *Klebsialla I*(17), and *Streptococcus*(18). These bacteria in tumors contribute to treatment (10–14); for example, *Gammaproteobacteria* found in pancreatic cancer induce

resistance to the widely used chemotherapeutic drug gemcitabine(10). Antibiotic treatment was associated with the efficacy of gemcitabine in mice(10) and in the clinic (19, 20). On the other hand, PDAC long-term survivors displayed diverse tumor microbes and immune activation (13). Moreover, aggressive tumors harbor distinctive microbial communities (8).

Despite the roles of intratumoral bacteria, the mechanisms of bacterial migration into pancreatic tumors are poorly understood. A mechanistic understanding of bacterial migration from the duodenum into the pancreas is critical for understanding pancreatic disease and thus improving therapeutic outcomes. Previous findings demonstrated that bacterial DNA profiles in the pancreas of the same subjects were similar to those in the duodenum tissue(21). In addition, orally administered *E. coli* was found in pancreatic tumors in mice (12), implying migration from the duodenum to the pancreas (figure 1**a**, b).

Literature about mathematical modeling and experimental studies of bacterial penetration in the gastrointestinal tract

Mathematical modeling of bacterial penetration in the human gastrointestinal tract is missing in the literature. Bacterial penetration into meat and leafy vegetables with sessile drops were mathematically modeled previously (22–24). Bacterial migration in colon mucus and to the epithelial layer was investigated(25). The effect of chemotaxis on host infection and pathogenicity was also reviewed (26). On the other hand, upstream swimming of *Escherichia coli* was analyzed (27–29). Diao and coworkers developed a three-channel microfluidic device to analyze bacterial chemotaxis(30).

Missing mechanistic understanding

Despite the aforementioned advances, a mechanistic understanding of the migration of aerobic bacteria from the duodenum into the pancreas with tumors has not been achieved. In particular, since bacterial invasion from the intestine into the pancreas is inhibited by defense systems such as bile flow and the high-pressure zone at the sphincter of Oddi, a muscle situated at the junction

of the duodenum and pancreatic duct (31) (figure 2), it has been unclear what factor makes a difference in bacterial migration into heathy pancreas and pancreas with tumors.

Objectives of this work

The hypotheses of this work are twofold: (1) migration of aerobic bacteria from the duodenum into the pancreas is explained by a mathematical model that includes bacterial random motility, the flow of pancreatic juice and bile, pH taxis, aerotaxis to higher oxygen and away from carbon dioxide, and (2) bacterial migration from the duodenum to the pancreas in the hepatopancreatic duct is experimentally modeled in a T-shaped cylinder, mimicking the pancreatic duct. This work first provides simulated migrations of aerobic bacteria from the duodenum to the pancreas with tumors. Second, the pH-tactic behaviors of *GFP E. coli* were demonstrated in a pH-gradient reproducible microfluidic device. Finally, pH-tactic migrations of *P. fluorescens* from the duodenum to pancreas were measured to validate the models. This work aims to understand how each factor and its combination with others contribute to the migration of aerobic bacteria from the duodenum to the pancreas with tumors.

Results

Migration of aerobic bacteria from duodenal fluid into the pancreas is driven by pH taxis

The simulated pH in the hepatopancreatic duct increased greatly from the duodenum with lower pH to the pancreas at neutral or slightly alkaline pH (figure 3 green, eqn. 17) since the diffusion of gastric acid into the hepatopancreatic duct is not just counteracted by bile and pancreatic juice flow but also neutralized by bicarbonate in pancreatic juice (eqn. 17) (figure 3). Carbon dioxide is generated as a byproduct of neutralization at the duodenum (eqn. 17) (figure 3 blue). The simulated pH in the pancreas at 7.6 (figure 4 green) agrees reasonably well with the literature that pancreatic juice has a pH of 8.0- 8.3 and liver bile has pH at 7.8 (38).

The migration of aerobic bacteria in the hepatopancreatic duct from the duodenum into the pancreas was simulated (Figures 4, 7, 1S). Factors that influence bacterial transport are

summarized in Table 1. The simulated bacterial concentration in the healthy pancreas (figure 4 blue) was lower than that in the literature (figure 4 orange)(12). However, the bacterial amount estimated using the typical weight of the pancreas at 80 g at 3.2 CFU seems consistent with the literature that 15% of healthy pancreas contained detectable bacteria (10). Bacteria did not migrate into the pancreatic duct due to motility alone, even at the periphery of duct, where fluid flow velocity is lower (Figure S1**b** black dotted). However, bacterial pH-taxis under the pH-gradient at the T-junction (figure 3 green) facilitates migration from acidic duodenum fluid toward pancreatic duct containing pancreatic juice at slightly alkaline pH, more favorable for them (figures S1**a**, **b** blue and green). Moreover, migration was slightly facilitated by aerotaxis of aerobic bacteria away higher carbon dioxide concentrations at the duodenum (Figures 3 blue, S1**b** blue and red).

Measured migration of GFP E. coli under a pH gradient in a microfluidic device validates pH taxis

A steady pH gradient was generated in a two-laminar flow-based PDMS microfluidic device (figure 5**a**), where the pH changed from 5–5.5 on the top to 8–9 at the bottom (figures 5**a**, S2). As a control, GFP *E. coli* migrated little without a gradient (figure 5**d**, **e** black). Under this pH gradient, the pH-tactic behaviors of *GFP E. coli* were analyzed (figure 5). When GFP *E. coli* were included under the pH gradient (figure 5a) in either the upper (figure 5**b**) or bottom inlets (figure 5**c**)*, GFP E. coli* migrated vertically from the upper channel with a lower pH toward the lower channel with a slightly alkaline pH (figures 5**b**, **c**, **e** blue and orange), showing pH-tactic behaviors. Note that carbon dioxide was generated at the top channel (0.7 mmol l^{-1}) due to neutralization (figure S3), where *E. coli* was attracted toward higher carbon dioxide (32). Thus, a higher bacterial concentration in the lower channel, where the carbon dioxide concentration is lower (Figures 5**b**, **c**, orange and green, S3), still assures pH taxis.

Measured upstream migration of P. fluorescens in a T-shaped cylinder validates the models

Upstream migrations of *Pseudomonas fluorecens* in a four-millimeter T-shaped cylinder against the flow of bicarbonate at 20 µl/min, in equilibrium to 5% carbon dioxide (figure S4), were measured to validate the models (movie S1). *Pseudomonas fluorescens* was chosen here, as *Pseudomonas*

was one of the most commonly found strains in pancreatic cancer (10) and can be seen under UV light using their intrinsic fluorescence. A lower flow rate of 20 µl/min was chosen to easily observe bacterial migration under flow conditions. *P. fluorescens* migrated upstream against bicarbonate flow with a maximum fluid velocity of 52 µm/s from hydrochloride solution at pH 5–6, with advancing velocity of approximately 60 µm/s (figure 6, S5**a,** movies S1 and 2 left). These upstream migrations of *P. fluorescens* are caused by pH taxis at the T-junction, where pH increases dramatically (figure 8**a**), pushing them from acidic areas toward neutral or slightly alkaline pH. This pH taxis wanes fluid flow in the cylinder, probably near the wall, where fluid velocity is lower (movies S1 and S2 left). Migration immediately close to the T-junction is swift, probably due to a greater pH and CO_2 gradient (figure 6a), compared with lower advancement in the areas far from the junction (figure 6**a**, S5**a**, movies S1 and S2 left). *P. fluorescens* in bicarbonate did not migrate against flow due to motility alone (figure S5**b**, movie S2 right). These results are consistent with the simulation results (Figure S6, movies S3 and 4).

Obstructed pancreatic and bile ducts in the pancreas with tumors increase migration

The simulated bacterial concentration in the pancreas with tumors (figure 4 gray) was over 100 times higher than that in the healthy pancreas (figure 4 blue) and agreed reasonably well with the literature (figure 4 yellow). This is also consistent with findings that 83% of pancreatic tumors contained detectable bacteria(10). Pancreatic ductal adenocarcinoma (PDAC), which occurs at the pancreatic duct, compresses the pancreatic duct, reducing pancreatic juice flow rates (33–35). Moreover, 70% of pancreatic cancer patients have biliary obstruction at the time of diagnosis (36, 37). The reduced pancreatic juice and bile flow rates led to easier migration toward the pancreas (Figures 7 and S7). In addition, the bacterial concentration in the pancreas with tumors was ellipse-

157 shaped with a lower concentration along the pancreatic duct and a higher concentration along the
158 duodenum wall due to reflux of bacteria to the duct (figure S7).
159
160 A*erotaxis of aerobic bacteria to higher oxygen at the duodenum affects migration less*
161 Oxygen dissolved in duodenal fluid diffuses into both the hepatopancreatic duct and duodenal wall
162 toward the pancreas with the tumor, where the oxygen concentration is lower, due to oxygen
163 consumption by cancer cells (figure S8). Note that diffusion in the duct is inhibited by flow, while
164 that in the duodenum wall is not inhibited but by the physical barrier of the wall (figure S8). Oxygen
165 in the duodenal wall surrounding the hepatopancreatic duct diffuses into the duct through the wall
166 of the duct (eqn. 5) (figure S8). Aerotaxis of aerobic bacteria toward the duodenum with higher
167 oxygen (figure S8) had little effect on migration (figure S9). This is probably because aerotaxis to
168 higher oxygen at the duodenum is outweighed by both aerotaxis away from higher carbon dioxide
169 concentration and pH-taxis to neutral pH in the pancreas (figure S9). Thus, aerobic bacteria,
170 showing aerotaxis to higher oxygen, even migrated into the pancreas with the tumor (figure S9
171 blue).
172
173 *Parametric sensitivity analysis*
174 Maximum fluid velocity greatly affects bacterial migration into the pancreas (figure 8). The pH of
175 duodenal fluid also has a great effect on migration into the pancreas since increased pH reduces
176 the pH gradient between the duodenum and pancreatic duct, which in turn reduces pH tactic-driven
177 migration (figure 8). The random motility coefficient has no effect on penetration, although the pH-
178 tactic sensitivity coefficient greatly affects penetration (figure 8). Increased permeability of the
179 hepatopancreatic duct also increased migration to the pancreas by increasing efflux from the duct
180 to pancreatic tissues (figure 8).
181
182 **Discussion**
183 *Factors contributing to faster pH-tactic velocity*

184 The measured pH-tactic velocity in a T-shaped cylinder is over 50 μm/s (figure 6b, S5b), much
185 faster than the typical chemotactic velocity at 10 μm/s. This may be due to the following reasons.
186 First, the gradient under flow is made greater since the flow inhibits diffusion (figure 3 green).
187 Second, an increase in pH leads to exponential decreases in hydrogen ion concentration. Thus,
188 chemotactic (pH-tactic) velocity (Keller-Segel model, eqn. 9), influenced by the concentration
189 gradient, is faster. Note that the hydrodynamic properties of bacteria such as rod-shaped *E. coli*
190 may also contribute to faster upstream migration than simulated bacteria (27).
191
192 *Pathway for migration of aerobic bacteria to pancreatic tumors*
193 The probable pathway for migration of aerobic and motile bacteria in the duodenum into the
194 pancreatic tumor is divided into the following four: (i) at the T-junction of duodenum and pancreatic
195 duct, i.e., high pressure zone of the Sphincter of Oddi, driven by pH-taxis under a sharp pH-gradient
196 (figures 3 green, 6**a,** 7), (ii) in the hepato-pancreatic duct, driven by pH-taxis under a milder gradient
197 (figure 3, 6**a**, 7), (iii) through the ductal wall out to pancreatic tissues (figure 7 and S2), (iv) in
198 pancreatic tissue (interstitium) and tumor (figure 7, S7). The first step is made easier in cancer
199 patients with obstructions of the bile and pancreatic duct by reducing flow velocity. The second step
200 is in the duodenum wall. The third step is probably driven by the concentration difference between
201 the duct and the interstitium (eqn. 6). The last step is migration in tissues, where bacterial motility
202 is inhibited by the geometric barrier of the interstitium (porous medium) but not by the flow. As a
203 result, bacterial motility in tumors is reduced due to densely packed interstitium (40). Note that
204 bacteria in healthy tissues are probably eliminated by the immune system, while those in tumors
205 are not due to the suppressed immune system (41).
206
207 *Origins of bacteria in pancreatic tumor*
208 These results may help controversy over the origins of bacteria found in pancreatic tumors. The
209 proposed origin in the literature includes the duodenum via the pancreatic duct and large intestine
210 through the portal vein (11). It is noteworthy that pancreatic cancer contains immotile bacteria
211 (Table S1), which do not show motility or pH-taxis, or migrate into the pancreas even in the reduced

flow (Figure 7). Thus, the latter route is not neglected. Moreover, the intestinal barrier in patients with obstructive jaundice is impaired, which is frequently accompanied by pancreatic cancer(36); thus, bacterial translocation via the bloodstream is promoted (42). On the other hand, bacterial colonization in the pancreas was not detected in a mouse model with defective intestinal permeability with increased permeability by *Campylobacter* infection (5). However, *Pseudomonas putida,* which is motile and highly aerobic, was the most common strain in pancreatic tumors (10) (Table S1), with a higher presence of *Pseudomonas* in cancer patients (21), which agrees with results showing that aerobic bacteria migrate upstream in the hepatopancreatic duct toward the pancreas with pH taxis (figures 6, 7, S5).

This mechanistic understanding is relevant to all possible transport phenomena between duodenum and pancreas, such as a link between oral microbiome and risk of pancreatic cancer (3, 4, 43, 44), roles of bacteria in carcinogenesis (7, 8), bacterial infection on common bile duct (37) and in pancreas with pancreatitis and its association with cancer risk (6), and bacteria in pancreatic tumor affecting chemo- or immunotherapy (10, 12)(figure 9). For example, possible entry of oral bacteria in the duodenum into the healthy pancreas (figure S1) is associated with cancer risk (3, 4, 43, 44). Moreover, our results are also relevant to migration routes into the pancreas with pancreatitis (6). The hypothetical mechanisms for migration to pancreas with pancreatitis in literature include hematogenous route via the circulation, transmural migration through the colonic bowel wall either to the pancreas (translocation), via the biliary duct system, and from the duodenum via the main pancreatic duct. (6). On the other hand, pancreatitis is followed by insufficiency of bicarbonate secretion (6), leading to greater gastric acidification(45). Acidified duodenum increases the pH gradient between the duodenum and the pancreas and thus migration (figure 8). This is also consistent with the literature that most bacteria in the pancreas with pancreatitis are aerobic (or facultative anaerobes), which prefer aerobic conditions in the duodenum. On the other hand, compressed pancreatic and bile ducts are probably attributed to solid stress of tumors due to dense extracellular matrix of fibrillary collagen and swelling hyaluronan (46, 47). On the other hand, reducing bacterial migration into the pancreas with tumors (figure 8)

may help antibiotic strategies improve the efficacy of gemcitabine(10,19, 20). Moreover, clinical translation of the fecal microbial transplant (FMT) strategy to directly or indirectly influence the tumor microbiome(17, 48) might benefit.

3. Conclusion

A mechanistic understanding of bacterial migration from the duodenum into the pancreas is provided (figure 10). The migration of bacteria into the pancreas in the hepatopancreatic duct seems to depend on a balance between pancreatic juice and bile flow in the duct as convection (this reduces migration) and bacterial pH taxis away from the duodenum with a lower pH toward the pancreas at neutral or slightly alkaline pH. An imbalance of this (for example, reduced flow in tumor) leads to increased migration. Mathematical modeling predicted bacterial migration into the pancreas with tumors. The simulated bacterial concentration in the pancreas with tumors agreed reasonably well with the literature. The pH-tactic behaviors from acidic areas toward neutral pH were validated in a microfluidic study. The mathematical models were further validated by measuring upstream migrations of bacteria under flow conditions.

4. Mathematical modeling of migration of aerobic bacteria from the duodenum to the pancreas with tumors

Transports of bacteria and oxygen, bicarbonate, carbon dioxide, and hydrogen ion with reactions in the hepatopancreatic duct were mathematically modeled. An anatomical schematic of the upper gastrointestinal tract modeled is described in figures 1a and 1b. The geometry of the axisymmetric cylindroid was used for hepatopancreatic duct, duodenum walls, and pancreas tissues (figure 1c). Aerobic bacteria favoring neutral pH, such as *Pseudomonas,* were used, as they are typically bacterial strains found in pancreatic cancer(10). A list of the factors included in

the modeling is shown in Table 1. The details of the modeling follow. The parameter list is provided in Table S2.

4.1 Migration of aerobic bacteria from the duodenum to the pancreas

Migration of aerobic bacteria from the duodenum to the pancreas is mathematically modeled using a diffusion-advection equation that includes bacterial motility, aerotaxis to oxygen, aerotaxis away from carbon dioxide pH taxis, and pancreatic juice and bile flow (convection), as described in the following governing equation:

$$\frac{\partial b}{\partial t} = \underbrace{\mu_{eff}\left(\frac{\partial^2 b}{\partial x^2}+\frac{\partial^2 b}{\partial r^2}+\frac{1}{r}\frac{\partial b}{\partial r}\right)}_{\text{motility}} \underbrace{-\left\{\frac{\partial}{\partial x}\left(V_a^x b\right)+\frac{\partial}{\partial r}\left(V_a^r b\right)+\frac{1}{r}\left(V_a^r b\right)\right\}}_{\text{aerotaxis to oxygen}} \underbrace{-\left\{\frac{\partial}{\partial x}\left(V_c^x b\right)+\frac{\partial}{\partial r}\left(V_c^r b\right)+\frac{1}{r}\left(V_c^r b\right)\right\}}_{\text{aerotaxis away from carbon dioxide}}$$
$$\underbrace{-\left\{\frac{\partial}{\partial x}\left(V_{pH}^x b\right)+\frac{\partial}{\partial r}\left(V_{pH}^r b\right)+\frac{1}{r}\left(V_{pH}^r b\right)\right\}}_{\text{pH-taxis}} \underbrace{-\frac{\partial}{\partial x}\left(v_h b\right)}_{\substack{\text{bile and}\\ \text{pancreatic juice flow}}} \quad (1)$$

b [CFU ml^{-1}] is bacterial concentration, μ_{eff} [m^2 s^{-1}] is effective random motility coefficient of bacteria, V_a and V_c [m s^{-1}] is aerotactic velocity to oxygen and carbon dioxide, respectively, V_{pH} [m s^{-1}] is pH-tactic velocity, and v_h [m s^{-1}] is the fluid flow velocity in hepato-pancreatic duct. Superscripts of x and r indicate the direction of aerotactic and pH taxis. The growth term was not included here, as the period for bacterial migration (less than ten hours) is in general shorter than bacterial growth (>10 h). Aerobic bacteria that respire only in aerobic conditions with an oxygen substrate with carbon dioxide as a byproduct show aerotaxis to higher oxygen and toward lower carbon dioxide, which were modeled. Chemotactic terms are typically modeled in convective terms in the Keller-Segel model (50). A simplified one-dimensional model of eqn. 1 is provided in supporting information. Each term will be described below in depth.

4.1.1 Random motility of bacteria

Motile bacteria show diffusion-like random motion of run-and-tumble motility using their flagellar. Bacterial motility is described in a diffusive term using the effective random motility coefficient, μ_{eff} [$m^2\ s^{-1}$], as:

$$v_{motility} = -\mu_{eff}\frac{\partial b}{\partial x} \quad (2)$$

The effective random motility coefficient is dependent on the viscosity of the fluid in the hepatopancreatic duct, η_h [mPa·s], and is described as follows(23):

$$\mu_{eff} = \mu_0\left(\frac{\eta_w}{\eta_h}\right)^2 \quad (3)$$

η_w [mPa·s] is the viscosity of water. Therefore, the viscosity in the hepatopancreatic duct should be lower than that in bile or pancreatic juice as they are diluted there, as calculated using the viscosity of pancreatic juice, η_p [mPa·s], pancreatic juice flow, U_p [ml min^{-1}] and bile flow rate, Q_b [ml min^{-1}] as:

$$\eta_h = \frac{Q_p}{Q_p + Q_b}\eta_p \quad (4)$$

This is based on the assumption that pancreatic juice and bile acid contribute to viscosity independently. This is justified as pancreatic juice viscosity is due to enzymatic proteins, while the viscous contribution of bile is due to bile acids. Using parameters of viscosity of pancreatic juice of 1.5 mPa·s(51), bile flow rate at 0.43 ml min^{-1}, and pancreatic juice flow rate at 0.2 ml min^{-1} (table S2), the viscosity due to pancreatic juice is at 0.95 mPa·s (eqn. 4). The viscosity of bile at 0.90 mPa·s(52) is lower than that (0.95 mPa·s). Thus, a viscosity of 0.95 mPa·s is used for that in the hepatopancreatic duct. Pancreatic tissues are considered porous media, and the random

motility coefficient in pancreatic tissues is described using tortuosity τ [-] and porosity ϕ [-] as follows:

$$D_{eff}^{O_2} = D_0^{O_2} \frac{\eta_w}{\eta_h} \cdot \frac{\phi}{\tau} \ (0 < r < r_h) \quad (5)$$

Bacterial transport across the wall of the duct is described using permeability of the duct of bacteria, P_b [m s^{-1}] as follows:

$$Flux_b\left(r = r_h\right) = P_b\left\{b\left(r = r_h\right)_{wall} - b\left(r = r_h\right)_{duct}\right\} \quad (6)$$

where $b(r = r_h)_{wall}$ and $b(r = r_h)_{duct}$ are bacterial concentrations on the ductal wall in the duodenum wall and hepatopancreatic duct, respectively. r_h [mm] is the radius of the hepato-pancreatic duct. Note the unit of flux is CFU m^{-2} s^{-1}. The permeability of the bile duct for bacteria was determined from measurements in rats in the literature. The permeability of the human bile duct is estimated using a bile duct wall thickness of 80 μm in mice(53) and that in humans at 0.5 mm(54) .

4.1.2 Aerotaxis

Bacteria monitor their cellular energy levels and respond to a decrease in energy by swimming to a microenvironment that reenergizes the cells(55). Thus, bacteria migrate toward optimal oxygen and carbon dioxide levels for better energy production by using a strategy called "energy taxis" (56). Additionally, carbon dioxide also works as an attractant or repellent, although less is known about this. Adult *Caenorhabditis elegans* display an acute avoidance response upon exposure to CO_2 (57, 58). The facultative anaerobe *Oscillatoria* migrated away from air to carbon dioxide (32).

In aerotaxis, bacteria use sensing mechanisms called 'logarithmic sensing,' where bacteria sense the logarithm of the concentration gradient(59). A modified Keller-Segel model, Lapidus and Schiller model(60), is used for logarithmic sensing of the aerotactic term for oxygen in Eqn. (7):

$$V_a^x = \chi_0^a \frac{K_d}{\left(K_d + a\right)^2} \cdot \frac{\partial a}{\partial x} \tag{7}$$

where a [mol l^{-1}] is the oxygen concentration, χ_0^a [m^2 s^{-1}] is the chemotactic sensitivity coefficient of bacterial aerotaxis, and K_d [mmol l^{-1}] is the dissociation constant. Note that aerotactic velocity is independent of viscosity(61). Aerotaxis away from higher carbon dioxide is described in:

$$V_c^x = -\chi_0^c \frac{1}{\left(K_d^c + c\right)} \cdot \frac{\partial c}{\partial x} \tag{8}$$

K_d^c [mmol/] is the dissociation constant for the ligand and receptor for carbon dioxide. A typical chemotactic sensitivity coefficient of 1 x 10^{-8} m^2 s^{-1} is used.

4.1.3 pH-taxis

Bacteria that grow optimally in a pH range of near neutral (bacteria) require robust mechanisms for cytoplasmic pH homeostasis to survive and, in some cases, grow during exposure to acidic or alkaline conditions that are well outside the pH range tolerated for cytoplasmic pH(62–64). A sensing mechanism is called 'pH taxis', a bidirectional behavior that migrates away from extremely acidic and alkaline environments and to optimal pH.

A continuum-based mathematical model for bacterial pH taxis is developed here based on a traditional chemotaxis Keller-Segel (K-S) model. Chemotactic velocity, V_c [m/s], is proportional to the logarithm of the chemoattractant (or chemorepellent) concentration gradient, as described in

$V_c = \chi / c \cdot \partial c / \partial x$, where c [mol/l] is the chemoattractant or chemorepellent concentration and χ [$m^2\ s^{-1}$] is the chemotactic sensitivity coefficient. However, this equation cannot be applied to pH taxis, as pH-tactic bacteria exhibit bidirectional behavior, i.e., away from alkaline and acidic pH toward neutral pH. Therefore, we modified the K-S model so that bacteria can sense the logarithm of "differences of concentration from optimal concentration", as described in the following:

$$V_{pH}^{x} = \chi_0^{pH} \frac{d\left(\ln([H^+] - [H^+]_0)\right)}{dx} = \chi_0^{pH} \frac{1}{\left([H^+] - [H^+]_0\right)} \cdot \frac{d\left([H^+]\right)}{dx} \quad (9)$$

where $[H^+]_0$ is the optimal hydrogen ion concentration for bacteria, $[H^+]$ is the hydrogen ion concentration, and χ_0^{pH} [$m^2\ s^{-1}$] is the pH-tactic sensitivity coefficient.

This model was validated against the measured distribution of *Serratia marcescens* under a pH gradient by Zuang and coworkers with their permissions(63). Motility and pH-tactic contributions were calculated from the difference in distribution density of bacteria for motility contribution and eqn. (5) for pH-taxis, respectively. The optimal pH for *S. marcescens*, pH_0 at 7.2, is used from the study. In the steady state, the ratio of motility to pH-taxis contribution is constant, as described in the following equation:

$$\underbrace{\frac{db}{dx}}_{\text{motility contribution}} = -\frac{\chi_0^{pH}}{\mu} \cdot \underbrace{\frac{1}{\left([H^+] - [H^+]_{opt}\right)} \cdot \frac{d\left([H^+]\right)}{dx} b}_{\text{pH-tactic contribution}} \quad (10)$$

This equation is obtained from eqn. (1) for the one-dimensional case without flow (v = 0) or aeortaxis ($\chi_0^{aero} = 0$). The motility and pH-tactic contribution calculated from data in the literature are shown in Figure S12 when the probability density of bacteria, ρ, was used in place of b in eqn. (10). The contribution of motility was reasonably well correlated with the pH-taxis

367 contribution in the literature (63) with correlation coefficients of 0.89 and 0.91 for pH < 7.2 and pH
368 > 7.2 (figure S12), validating the model. The parameter of the chemotactic sensitivity coefficient,
369 χ_0^{pH} [m^2 s^{-1}], was calculated from the slope of Figure S12, *k*, which is equal to the ratio of the
370 chemotactic sensitivity coefficient to the random motility coefficient from Eqn. (10):

371 $$k = \frac{\chi_0^{pH}}{\mu_0} \tag{11}$$

372 These coefficients, *k*, are 65.1 and –35.2 for pH < 7.2 and pH > 7.2, respectively. From a given
373 random motility coefficient, the chemotactic sensitivity coefficient of pH taxis is determined.

374 *Ion equilibrium and transport*

375 Pancreatic juice contains bicarbonate, HCO_3^-, at approximately 80 mmol l^{-1} in the fasted
376 state(65), and this bicarbonate neutralizes gastric acid in the duodenum in the following two
377 equilibrium equations:

378 $$H^+ + HCO_3^- \rightleftarrows H_2CO_3 \tag{12}$$

379 $$H_2CO_3 \rightleftarrows H_2O + CO_2 \tag{13}$$

380 These reactions can be written in a single equilibrium equation:

381 $$H^+ + HCO_3^- \underset{k-}{\overset{k+}{\rightleftarrows}} H_2O + CO_2 \tag{14}$$

382 Equilibrium equations in eqns. (12) and (13) are described using dissociation constants K_1 [mol l^{-}
383 ^{1}] and K_2 [-]:

384 $$\frac{[H^+][HCO_3^-]}{[H_2CO_3]} = K_1 \tag{15}$$

385 $$\frac{[H_2CO_3]}{pCO_2} = K_2 \tag{16}$$

These are summarized in:

$$\frac{[H^+][HCO_3^-]}{pCO_2} = \frac{k_-}{k_+} = K_1 K_2 = K^* \tag{17}$$

K^* = $10^{-6.1}$ mol l^{-1} and k_- = 3.71 x 10^{-2} s^{-1} from the literature(66). Note eqn. (17) can be rewritten in a simple manner:

$$pH = pK^* + \ln \frac{[CO_2]}{[HCO_3^-]} \tag{18}$$

The transport of hydrogen ions in the duct is described with reaction terms as follows:

$$\frac{\partial [H^+]}{\partial t} = \underbrace{D_{eff}^{H+}\left(\frac{\partial^2 [H^+]}{\partial x^2} + \frac{\partial^2 [H^+]}{\partial r^2} + \frac{1}{r}\frac{\partial [H^+]}{\partial r} \right)}_{\text{diffusion}} \underbrace{-\frac{\partial}{\partial x}\left(u_h [H^+]\right)}_{\substack{\text{bile and} \\ \text{pancreatic juice flow}}} \underbrace{-k_+ [H^+][HCO_3^-] + k_- [CO_2]}_{\text{reactions}} \tag{19}$$

Diffusion across the ductal wall at $r = r_h$ is described using permeability as follows:

$$Flux_{H^+} = P_{H^+}\left([H^+]_{r=r_h}^{wall} - [H^+]_{r=r_h}^{duct} \right) \tag{20}$$

where P_{H^+} [m s^{-1}] is the ductal permeability of hydrogen ions. $[H^+]_{r=r_h}^{wall}$ and $[H^+]_{r=r_h}^{duct}$ [mol l^{-1}] are the hydrogen ion concentrations on the ductal wall in the duodenum and hepatopancreatic duct, respectively. The concentrations of bicarbonate and carbon dioxide in the duct, $[HCO_3^-]$ and $[CO_2]$ [mol l^{-1}], are also described in the same manner as:

$$\frac{\partial [HCO_3^-]}{\partial t} = \underbrace{D_{eff}^{HCO3-}\left(\frac{\partial^2 [HCO_3^-]}{\partial x^2} + \frac{\partial^2 [HCO_3^-]}{\partial r^2} + \frac{1}{r}\frac{\partial [HCO_3^-]}{\partial r} \right)}_{\text{diffusion}} \underbrace{-\frac{\partial}{\partial x}\left(u_h [HCO_3^-]\right)}_{\substack{\text{bile and} \\ \text{pancreatic juice flow}}} \underbrace{-k_+ [H^+][HCO_3^-] + k_- [CO_2]}_{\text{reactions}} \tag{20}$$

$$\frac{\partial [CO_2]}{\partial t} = \underbrace{D_{eff}^{CO2}\left(\frac{\partial^2 [CO_2]}{\partial x^2} + \frac{\partial^2 [CO_2]}{\partial r^2} + \frac{1}{r}\frac{\partial [CO_2]}{\partial r} \right)}_{\text{diffusion}} \underbrace{-\frac{\partial}{\partial x}\left(u_h [CO_2]\right)}_{\substack{\text{bile and} \\ \text{pancreatic juice flow}}} \underbrace{+k_+ [H^+][HCO_3^-] - k_- [CO_2]}_{\text{reactions}} \tag{21}$$

401

402 *4.1.4 Fluid flow velocity in the hepato-pancreatic duct*

403 The bile duct and pancreatic duct joints together at the distal pancreas, consisting of a
404 hepatopancreatic duct or common channel 1–11 mm in length(67,68), open in the duodenum.
405 Thus, fluid flow in the hepatopancreatic duct is caused by both bile and pancreatic juice. Bile and
406 pancreatic juice flow rates were calculated from daily total bile flow at 620 ml day^{-1} (0.43 ml min^{-1})(69), and the pancreatic juice flow rate during the fasted state was 0.2–0.3 ml min^{-1}. The flow
408 rate of a *fasted* period is used here, as migration should be more straightforward during this
409 period, when bile and pancreatic juice secretions are lower (70). Additionally, duodenal pH is
410 faster in the fasted period. The volumetric flow rate in the hepatopancreatic duct, Q_h [ml/min], is
411 thus calculated as follows:

412
$$Q_h = Q_p + Q_b \tag{22}$$

413 The Reynolds number in the hepatopancreatic duct was calculated using the following equation:

414
$$\mathrm{Re} = \frac{\rho Q_h}{\eta_h A} \tag{23}$$

415 A [m^2] is the cross-sectional area of the duct. The volumetric flow rate in the hepatopancreatic
416 duct of healthy individuals, Q_h [$m^3\ s^{-1}$], is 0.63 ml min^{-1}. Thus, the Reynolds number in the
417 hepatopancreatic duct was calculated to be 0.52, assuring laminar flow. Thus, the fluid velocities
418 follow the Hagen-Poiseuille law as:

419
$$v_h(r) = v_{\max}\left\{1 - \left(\frac{r}{r_h}\right)^2\right\} \tag{24}$$

420 $v_h(r)$ is the fluid velocity at the ductal radius of r [mm], and r_h [mm] is the radius of the
421 hepatopancreatic duct. The maximum flow velocity, v_{max} [m s^{-1}], is calculated as:

$$v_{\max} = \frac{2Q_h}{\pi r_h^{\,2}} \tag{25}$$

The maximum flow velocity in the hepatopancreatic duct for a *healthy* individual is 494 μm s^{-1}. The pancreatic juice flow rate of pancreatic cancer patients is 1/4 that of healthy individuals in the literature(21. The flow rate of bile for cancer patients is missing in the literature. Therefore, the flow rate of patients with obstruction due to bile stones at 56 – 373 ml/day (212 ml/day on average) (71is used for cancer patients. The maximum flow rate in the duct for cancer patients is calculated at 126 μm s^{-1}.

4.2 Oxygen transport

Oxygen transport in the hepatopancreatic duct, duodenal wall, and pancreatic tissues is mathematically modeled and includes diffusion and flow in the hepatopancreatic duct, as described in the following equation:

$$\frac{\partial a}{\partial t} = \underbrace{D_{eff}^{O_2}\left(\frac{\partial^2 a}{\partial x^2} + \frac{\partial^2 a}{\partial r^2} + \frac{1}{r}\frac{\partial a}{\partial r}\right)}_{\text{diffusion}} \underbrace{-\frac{\partial}{\partial x}\left(v_h a\right)}_{\substack{\text{bile and} \\ \text{pancreatic juice flow}}} \tag{26}$$

where a [mol l^{-1}] is the oxygen concentration, D_{eff}^{O2} [m^2 s^{-1}] is the effective diffusion coefficient of oxygen in the hepatopancreatic duct, and pancreatic tissues are considered porous media. The effective diffusion coefficient of oxygen is thus described as:

$$D_{eff}^{O_2} = D_0^{O_2}\frac{\eta_w}{\eta_h}\cdot\frac{\phi}{\tau} \quad (0 < r < r_h) \tag{27}$$

D_0 [m^2 s^{-1}] is the diffusion coefficient of oxygen in water at 37°C, η_w [mPa·s] is the viscosity of water, η_h [mPa·s] is the viscosity of fluid in the hepatopancreatic duct, ϕ [-] is porosity and τ [-] is tortuosity. Therefore, the flux of oxygen across the hepatopancreatic duct is also described as follows:

443 $$Flux = P_{O2}\left(a^{wall}_{r=r_h} - a^{duct}_{r=r_h}\right) \quad (28)$$

444 Oxygen transport is not included in the healthy pancreas, assuming no oxygen concentration
445 difference between healthy pancreas and duodenum, but was included for transport in the
446 pancreas with tumor since oxygen concentration in the pancreatic tumor is lower due to rapid
447 oxygen consumption by cancer cells.

448

449 4.3 Boundary conditions and numerical simulations

450 The governing equations were numerically solved using COMSOL Multiphysics 5.0 with initial and
451 boundary conditions as follows. The bacterial concentration in duodenum fluid at 10^4 CFU ml^{-1}
452 was used for the boundary condition(72:

453 $$b\left(x=0\right) = 10^4 \text{ CFU ml}^{-1} \quad (28)$$

454 The oxygen concentration in the human duodenum is not available in the literature. The oxygen
455 concentration in the stomach is 58 mmHg in mice, while that in the duodenum is 32 mmHg(73)
456 Oxygen level in the human stomach is at 15–16% (74). Using this ratio of oxygen concentration in
457 mice and equilibrium the oxygen concentration to air at 37°C at 0.21 mmol l^{-1}, oxygen
458 concentration in duodenum at 0.083 mmol l^{-1} is used. Oxygen concentration in tumors at 15
459 mmHg is also used(75)

460 $$a\left(x=0\right) = 0.083 \text{ mmol l}^{-1} \quad (29)$$

461 $$a\left(x=x_d\right) = 0.039 \text{ mmol l}^{-1} \quad (30)$$

462 The distance between the duodenum and pancreatic tumor did not affect the oxygen
463 concentration gradient between the duodenum and the pancreatic tumor in preliminary simulation
464 studies. The pH of fasted human duodenum at 4.9 is used (39)

$$pH(x=0)=4.9 \tag{31}$$

An initial carbon dioxide concentration of 5% (2.64 mmol/l) was used.

$$[CO_2]_0(t=0)=2.64\ \text{mmol/l} \tag{32}$$

The bicarbonate concentration in pancreatic juice during the fasting period is 80 mmol l^{-1} (57).

$$[HCO_3^-]_0(t=0)=80\ \text{mmol/l} \tag{33}$$

5. Experimental methods

5.1 Bacterial chemotaxis and pH taxis in a microfluidic device

A polydimethylsiloxane (PDMS) microfluidic device that can generate a steady concentration gradient using double-layered flow was fabricated (figure S12). PDMS elastomer base (SILPOT™ 184 Silicone Elastomer Base) was mixed with a curing agent (SILPOT™ 184 Silicone Elastomer Curing Agent) at a ratio of 10:1. The PDMS mixture was degassed using a vacuum chamber (G-20DA, ULVAC KIKO. Inc., Japan). The degassed mixture was poured onto the metal mold, designed for the device and created previously, and cured by heating at 75°C for two hours. Then, PDMS was peeled off of the metal mold. Both surfaces of the PDMS microfluidic device and a sliding glass were irradiated with oxygen plasma (SEDE-P, meiwafosis, Japan) at 10 pascals at 5 mA for 35 seconds. Both were attached to each other and heated at 90°C for one hour to permanently bond.

Preparation of bacteria

Pseudomonas fluorescens (ATCC 13525) and GFP *E. coli* (ATCC 25922™) were cultured in LB broth with stirring using a magnetic stirrer at 37°C at least overnight. *Pseudomonas fluorecens* was chosen here because *Pseudomonas* is one of the most common strains in pancreatic cancer(3), and they can be seen using their intrinsic fluorescence with UV excitation and emission at 340 nm(13). The obtained bacterial culture was centrifuged at 4,000 rpm for ten

minutes. The bacterial pellet was then washed in distilled water and centrifuged again. The pellet was then diluted into hydrochloride or bicarbonate solution.

Syringe pumps (Aladdin 1000, US) were connected to this microfluidic device. Bicarbonate (80 mmol/l) and hydrochloride (10^{-3} mol/l) solutions were poured at 200 µl/min from inlets 1 and 2, respectively (figure 2a). *GFP E. coli* were included in either of them. Bacterial distribution was measured from the fluorescence of *GFP E. coli* under irradiation with UV light (350 nm) using a digital single lens reflex (D5100, Nikon, Japan) in black-and-white mode. The pH in the microfluidic channel was visualized using bromothymol blue solution (figure 2a) or phenolphthalein solution (Sigma Aldrich, Japan) (figure S2). The obtained images were analyzed using ImageJ (NIH, US). The relative brightness was calculated as $(B_{max}-B)/(B_{max}-B_{min})$.

5.2 Upstream swimming of bacteria in different pH solutions against flow

Upstream migration of *Pseudomonas fluorescens* (ATCC 13525) from hydrochloride solution or sodium bicarbonate under bicarbonate solution flow was analyzed using a T-shaped cylinder fabricated by referring to previous literature(76). First, the degassed mixture of PDMS was poured into a 12-mm diameter petri dish with a thickness of a few millimeters (figure S15**a**). This PDMS mixture was cured at 75°C for two hours as a basis for the cylinder. Then, glass tubes were placed in T-shaped tubes, and another PDMS mixture was poured there (Figure S15**b, c**). The tubes were then removed carefully by incising with a cutter, leaving a hollow T-shaped cylinder (figure S15**d**). End tips of the hollowed cylinders were filled with remaining cured PDMS so that the PDMS that would be poured later would not be filled in. Finally, the PDMS mixture was poured into the whole device and cured (figure S15**e**).

Five-milliliter syringes filled with hydrochloride (approximately $10^{-4.9}$ mol/l) or sodium bicarbonate (80 mmol/l) solution containing bacteria were connected to the upper inlet of the T-shaped cylinder. Bacteria in hydrochloride solution were prepared by diluting the bacterial pellet obtained by centrifugation with hydrochloride at the desired concentration. The pH was adjusted by the

color of bromocresol purple (Wako Chem., Japan). This concentration of hydrochloride is chosen because that of fasted duodenum is at 4.9–5.5(39). The flow rates were 200 μl/min and 20 μl/min. The pH distribution was measured by bromocresol purple (FujifilmWako, Japan). Bacteria were measured in the same manner as Sec. 5.1, but movies were taken using a CMOS image sensor (IMX586, Sony, Japan). The obtained movies were analyzed using MATLAB 2021 (MathWorks, Japan), as shown in Figure S16. Horizontal distance in millimeters was calculated from a ruler in an image placed near the device.

Acknowledgments

This research is financially supported by the Keio Gijuku Academic Development Funds for multidisciplinary Research (2019). We acknowledge the provision of data for pH taxis by Prof. Mertin Sitti of the Max Planck Institute. We acknowledge discussions with Dr. Masayasu Horibe and Dr. Eisuke Iwasaki of School of Medicine, Department of Internal Medicine (Gastroenterology and Hepatology) of Keio University. We acknowledge the Keio University manufacturing center for creating the metal mold for the microfluidic device.

References

1. Rawla P, Sunkara T, Gaduputi V (2019) Epidemiology of Pancreatic Cancer: Global Trends, Etiology and Risk Factors. *World J. Oncol.* 10(1):10–27.
2. Gopalakrishnan V, et al. (2018) Gut microbiome modulates response to anti-PD-1 immunotherapy in melanoma patients. *Science,* 359(6371):97–103.
3. Gaiser RA, et al. (2019) Enrichment of oral microbiota in early cystic precursors to invasive pancreatic cancer. *Gut* 68(12):2186–2194.
4. Li, S., G.M. Fuhler, N. BN, T. Jose, M.J. Bruno, M.P. Peppelenbosch, and S.R. Konstantinov. (2017). Pancreatic cyst fluid harbors a unique microbiome. *Microbiome*. 5.

5. Lillioja S, Mott DM, Spraul M, Ferraro R, Foley JE, R.E. et al. (1993). *The New England Journal of Medicine*. Massachusetts Medical Society. All rights reserved. N. Engl. J. Med. 29: 1230–5.
6. Schmid, S.W., W. Uhl, H. Friess, P. Malfertheiner, and M.W. Büchler. (1999). The role of infection in acute pancreatitis. *Gut*. 45: 311–316.
7. Thomas, R.M. et al. (2018). Intestinal microbiota enhances pancreatic carcinogenesis in preclinical models. *Carcinogenesis*. 39: 1068–1078.
8. Guo, W., Y. et al. (2021). Tumor microbiome contributes to an aggressive phenotype in the basal-like subtype of pancreatic cancer. Commun. Biol. 4: 1–13.
9. Nejman D, et al. (2020) The human tumor microbiome is composed of tumor type-specific intracellular bacteria. *Science,* 368(6494):973–980.
10. Geller LT, et al. (2017) Potential role of intratumor bacteria in mediating tumor resistance to the chemotherapeutic drug gemcitabine. *Science*;357(6356):1156–1160.
11. Thomas RM, Jobin C (2020) Microbiota in pancreatic health and disease: the next frontier in microbiome research. *Nat Rev Gastroenterol Hepatol* 17(1):53–64.
12. Pushalkar S, et al. (2018) The pancreatic cancer microbiome promotes oncogenesis by induction of innate and adaptive immune suppression. *Cancer Discov* 8(4):403–416.
13. Riquelme E, et al. (2019) Tumor Microbiome Diversity and Composition Influence Pancreatic Cancer Outcomes. *Cell* 178(4):795-806.e12.
14. Chandra, V., and F. McAllister. (2021). Therapeutic potential of microbial modulation in pancreatic cancer. Gut. 70: 1419–1425.
15. Ezenobi NO, Okpokwasili GC (2016) Combined effect of temperature and pH on *Pseudomonas aeruginosa* isolated from a cosmetic product. *Int. J. Curr. Res.* 8(08):37124–37130.
16. Gunasekaran V, Kotay SM, Das D (2006) Alkaline lipase production by Citrobacter freundii IIT-BT L139. *Indian J Exp Biol* 44(6):485–491.
17. Abbas SZ, et al. (2014) Isolation and characterization of arsenic resistant bacteria from wastewater. *Brazilian J Microbiol* 45(4):1309–1315.

18. Beal C, Louvet P, Corrieu G (1989) Influence of controlled pH and temperature on the growth and acidification of pure cultures of Streptococcus thermophilus 404 and Lactobacillus bulgaricus 398. *Appl Microbiol Biotechnol* 32(2):148–154.
19. Nakano S, et al. (2020) Association between the use of antibiotics and efficacy of gemcitabine plus nab-paclitaxel in advanced pancreatic cancer. *Medicine (Baltimore)*
20. Imai H, et al. (2019) Antibiotic therapy augments the efficacy of gemcitabine-containing regimens for advanced cancer: A retrospective study. *Cancer Manag Res* 11:7953–7965.
21. Del Castillo E, et al. (2019) The microbiomes of pancreatic and duodenum tissue overlap and are highly subject specific but differ between pancreatic cancer and noncancer subjects. *Cancer Epidemiol Biomarkers Prev* 28(2):370–383.
22. Ranjbaran, M., and A.K. Datta. (2021). Engineering modeling frameworks for microbial food safety at various scales.: 1–37.
23. Shirai H, Datta AK, Oshita S (2017) Penetration of aerobic bacteria into meat : A mechanistic understanding. *J Food Eng* 196:193–207.
24. Ranjbaran, M., and A.K. Datta. (2019). Retention and infiltration of bacteria on a plant leaf driven by surface water evaporation. *Phys. Fluids.* 31: 112106.
25. Figueroa-Morales N, Dominguez-Rubio L, Ott TL, Aranson IS (2019) Mechanical shear controls bacterial penetration in mucus. *Sci Rep* 9(1):1–10.
26. Matilla MA, Krell T. The effect of bacterial chemotaxis on host infection and pathogenicity. *FEMS Microbiol Rev.* 2018 Jan 1;42(1).
27. Kaya T, Koser H (2012) Direct upstream motility in Escherichia coli. *Biophys J* 102(7):1514–1523.
28. Marcos, H.C. Fu, T.R. Powers, and R. Stocker. (2012). Bacterial rheotaxis. Proc. Natl. Acad. Sci. U. S. A. 109: 4780–4785.
29. Figueroa-Morales N, et al. (2020) E. Coli “supercontaminates” narrow ducts fostered by broad run-time distribution. *Sci Adv* 6(11):1–8.Marcos, Fu HC, Powers TR, Stocker R (2012) Bacterial rheotaxis. *Proc Natl Acad Sci U S A* 109(13):4780–4785.

30. Diao J, et al. (2006) A three-channel microfluidic device for generating static linear gradients and its application to the quantitative analysis of bacterial chemotaxis. *Lab Chip* 6(3):381–388.
31. Sung JY, Costerton JW, Shaffer EA (1992) Defense system in the biliary tract against bacterial infection. *Dig Dis Sci* 37(5):689–696.
32. G, Walsby AE (1985) Chemotaxis of a cyanobacterium on concentration gradients of carbon dioxide, bicarbonate and oxygen. *J Gen Microbiol* 131(10):2643–2652.
33. Rinderknecht H, Renner IG, Stace NH (1983) Abnormalities in pancreatic secretory profiles of patients with cancer of the pancreas. *Dig Dis Sci* 28(2):103–110.
34. Carr-Locke DL (1980) Serum and pancreatic juice carcinoembryonic antigen in pancreatic and biliary disease. *Gut* 21(8):656–661.
35. Gregg JA, Sharma MM (1978) Endoscopic measurement of pancreatic juice secretory flow rates and pancreatic secretory pressures after secretin administration in human controls and in patients with acute relapsing pancreatitis, chronic pancreatitis, and pancreatic cancer. *Am J Surg* 136(5):569–574.
36. Kruse EJ. Palliation in pancreatic cancer. Surg Clin North Am. 2010 Apr;90(2):355–64.
37. Muir CA (2004) Acute ascending cholangitis. *Clin J Oncol Nurs* 8(2):157–160.
38. Guyton AC. Human physiology and mechanism of disease. 1987: 499.
39. Ovesen L, et al. (1986) Intraluminal pH in the stomach, duodenum, and proximal jejunum in normal subjects and patients with exocrine pancreatic insufficiency. *Gastroenterology* 90(4):958–962.
40. Bhattacharjee, T., and S.S. Datta. (2019). Bacterial hopping and trapping in porous media. Nat. Commun. 10.
41. Westphal, K., S. Leschner, J. Jablonska, H. Loessner, and S. Weiss. Containment of tumor-colonizing bacteria by host neutrophils. *Cancer Res*. 68: 2952–2960.2008.
42. Abdeldayem, H., E. Ghoneim, A.A.-E. Refaei, and A. Abou-Gabal. Obstructive jaundice promotes intestinal-barrier dysfunction and bacterial translocation: experimental study. Hepatol. Int. 1: 444–448.2007.

625 43. Fan, X. et al. (2018). Human oral microbiome and prospective risk for pancreatic cancer: A
626 population-based nested case-control study. *Gut*. 67: 120–127.
627 44. Yoshida, H., M. et al. (2019). Coadministration of magnesium oxide reduces the serum
628 concentration of hydrophobic basic drugs in patients treated with antipsychotic drugs. *Biol.*
629 *Pharm. Bull.* 42: 1025–1029.
630 45. Bovo, P., G. et al. (1995). Intraluminal gastric pH in chronic pancreatitis. *Gut*. 36: 294–298.
631 46. Chauhan, V.P. et al. (2013). Angiotensin inhibition enhances drug delivery and potentiates
632 chemotherapy by decompressing tumor blood vessels. *Nat. Commun*. 4.
633 47. National Library of Medicine (U.S.). (2005, March - Fecal Microbial Transplants for the
634 Treatment of Pancreatic Cancer. Identifier NCT04975217.
635 48. Danino, T., A. et al.(2015). Programmable probiotics for detection of cancer in urine. Sci.
636 Transl. Med. 7.
637 49. Chowdhury, S. et al. (2019). Programmable bacteria induce durable tumor regression and
638 systemic antitumor immunity. Nat. Med. 25: 1057–1063.
639 50. Keller EF, Segel LA (1971) Model for chemotaxis. *J Theor Biol* 30(2):225–234.
640 51. Harada H, Ueda O, Kochi F, Kobayashi T, Komazawa M. Comparative studies on viscosity
641 and concentration of protein and hexosamine in pure pancreatic juice. *Gastroenterol Jpn.*
642 1981 Dec;16(6):623-6.
643 52. Reinhart WH, Näf G, Werth B (2010) Viscosity of human bile sampled from the common bile
644 duct. *Clin Hemorheol Microcirc* 44(3):177–182.
645 53. Smith D, Boyer L (1982) Permeability characteristics of bile duct in the rat. Am J Physiol.
646 Jan;242(1):G52-7.
647 54. Testoni PA, et al. (2006) Main pancreatic duct, common bile duct and sphincter of Oddi
648 structure visualized by optical coherence tomography: An ex vivo study compared with
649 histology. *Dig Liver Dis* 38(6):409–414.
650 55. Taylor BL, Zhulin IB, Johnson MS (1999) Aerotaxis and other energy-sensing behavior in
651 bacteria. *Annu Rev Microbiol* 53:103–128.

56. Taylor BL (1983) How do bacteria find the optimal concentration of oxygen? *Trends Biochem Sci* 8(12):438–441.
57. Bretscher AJ, Busch KE, De Bono M (2008) A carbon dioxide avoidance behavior is integrated with responses to ambient oxygen and food in Caenorhabditis elegans. *Proc Natl Acad Sci U S A* 105(23):8044–8049
58. Hallem EA, Sternberg PW (2008) Acute carbon dioxide avoidance in Caenorhabditis elegans. *Proc Natl Acad Sci U S A* 105(23):8038–8043.
59. Menolascina F, et al. (2017) Logarithmic sensing in Bacillus subtilis aerotaxis. *Npj Syst Biol Appl* 3(June):16036.
60. Lapidus IR, Schiller R (1976) Model for the chemotactic response of a bacterial population. *Biophys J* 16(12):779–789.
61. Schauer O, et al. (2018) Motility and chemotaxis of bacteria-driven microswimmers fabricated using antigen 43-mediated biotin display. *Sci Rep* 8(1):1–11. Krulwich TA, Sachs G, Padan E (2011) Molecular aspects of bacterial pH sensing and homeostasis. *Nat Rev Microbiol* 9(5):330–343.
62. Yang Y, Sourjik V (2012) Opposite responses by different chemoreceptors set a tunable preference point in Escherichia coli pH taxis. *Mol Microbiol* 86(6):1482–1489.
63. Zhuang J, Carlsen RW, Sitti M (2015) PH-taxis of biohybrid microsystems. *Sci Rep* 5:1–13.
64. Hu B, Tu Y (2014) Behaviors and Strategies of Bacterial Navigation in Chemical and Nonchemical Gradients. *PLoS Comput Biol* 10(6):e1003672.
65. Gerolami A, et al. (1989) Calcium Carbonate Saturation in Human Pancreatic juice: Possible Role of Ductal H+ Secretion. *Gastroenterology* 96(2):881–884.
66. Schulz KG, Riebesell U, Rost B, Thoms S, Zeebe RE (2006) Determination of the rate constants for the carbon dioxide to bicarbonate interconversion in pH-buffered seawater systems. *Mar Chem* 100(1–2):53–65.
67. Higashiyama H, et al. (2016) Anatomy of the Murine Hepatobiliary System: A Whole-Organ-Level Analysis Using a Transparency Method. *Anat Rec* 299(2):161–172.

679 68. Higashiyama H, et al. (2018) Anatomy and development of the extrahepatic biliary system in
680 mouse and rat: a perspective on the evolutionary loss of the gallbladder. *J Anat* 232(1):134–
681 145.
682 69. Esteller A (2008) Physiology of bile secretion. *World J Gastroenterol* 14(37):5641–5649.
683 70. Glasbrenner B, Dürrschnabel L, Büchler M, Malfertheiner P (1992) Nonparallel patterns of
684 circadian pancreatic and biliary secretions in fasting rats. *Int J Pancreatol* 11(3):169–177.
685 71. Ohya, T., Murakami, E., Kougame, A., Numata, Y., and Hiraoka, M. (2013). Proposal of
686 endoscopic lithotripsy for common bile duct stones based on the pathogenesis of stone
687 formation. C*holithiasis. Ann Surgery* 238 (1), 97-102 in Japanese.
688 72. Sender R, Fuchs S, Milo R (2016) Revised Estimates for the Number of Human and Bacteria
689 Cells in the Body. *PLoS Biol* 14(8):1–14.
690 73. He G, et al. (1999) Noninvasive measurement of anatomic structure and intraluminal
691 oxygenation in the gastrointestinal tract of living mice with spatial and spectral EPR imaging.
692 *Proc Natl Acad Sci U S A* 96(8):4586–4591.
693 74. Britannica Health & Medicine, Anatomy & Physiology Intestinal gas.
694 https://www.britannica.com/science/intestinal-gas Accessed Dec.18th, 2020.
695 75. Matsumoto S, et al. (2018) Metabolic and physiologic imaging biomarkers of the tumor
696 microenvironment predict treatment outcome with radiation or a hypoxia-activated prodrug in
697 mice. *Cancer Res* 78(14):3783–3792.
698 76. Pauty J, et al. (2018) A Vascular Endothelial Growth Factor-Dependent Sprouting
699 Angiogenesis Assay Based on an In Vitro Human Blood Vessel Model for the Study of Anti-
700 Angiogenic Drugs. *EBioMedicine* 27:225–236.
701 77. Spadoni, I., E. et al. (2015). A gut-vascular barrier controls the systemic dissemination of
702 bacteria. *Science*. 350: 830–834.
703
704

705 **Figures and Tables**

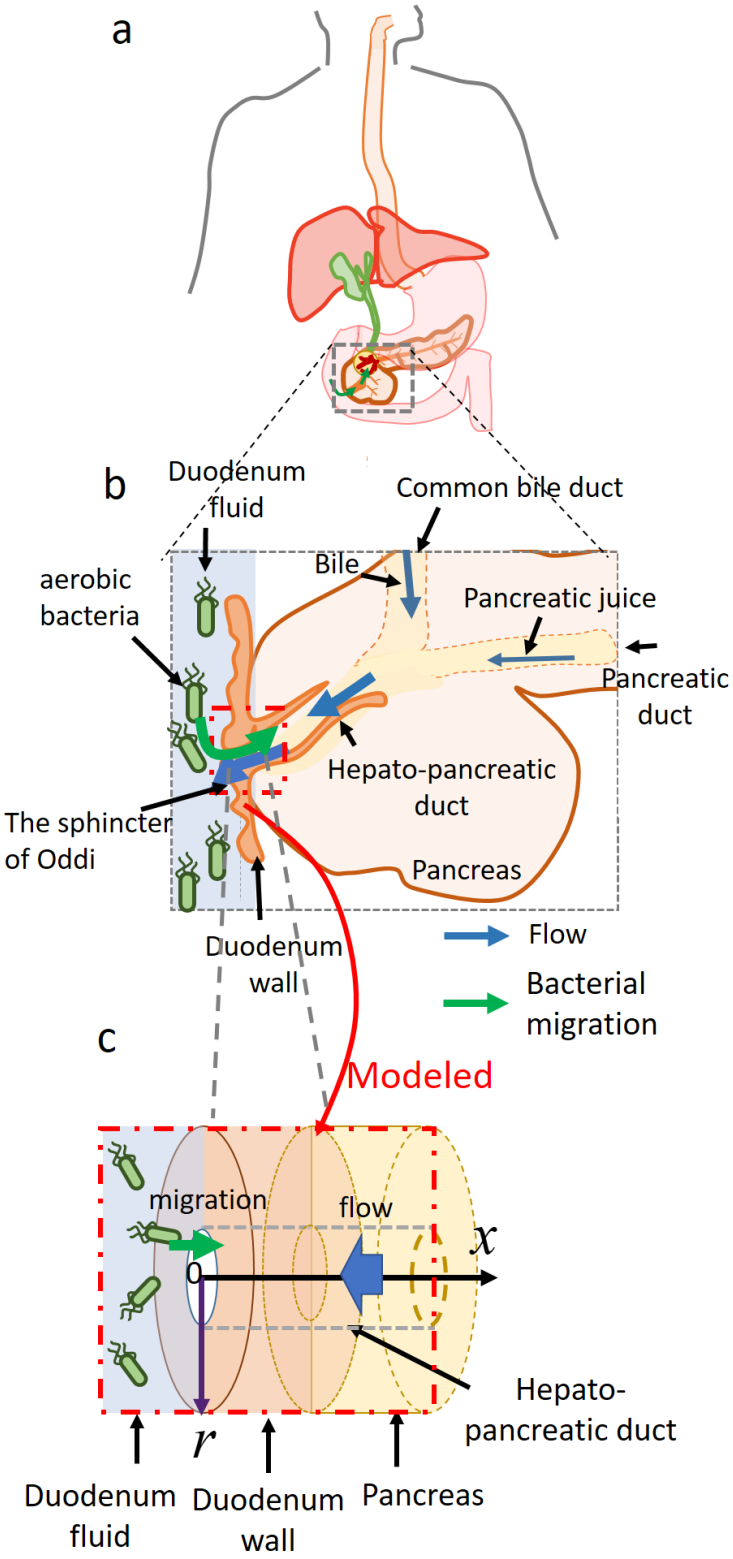

706

Figure 1. A schematic of the anatomy of the upper gastrointestinal tract (**a**) and a magnification of the duodenum and pancreas (**b**). **c**: Geometry used for mathematical modeling of bacterial migration.

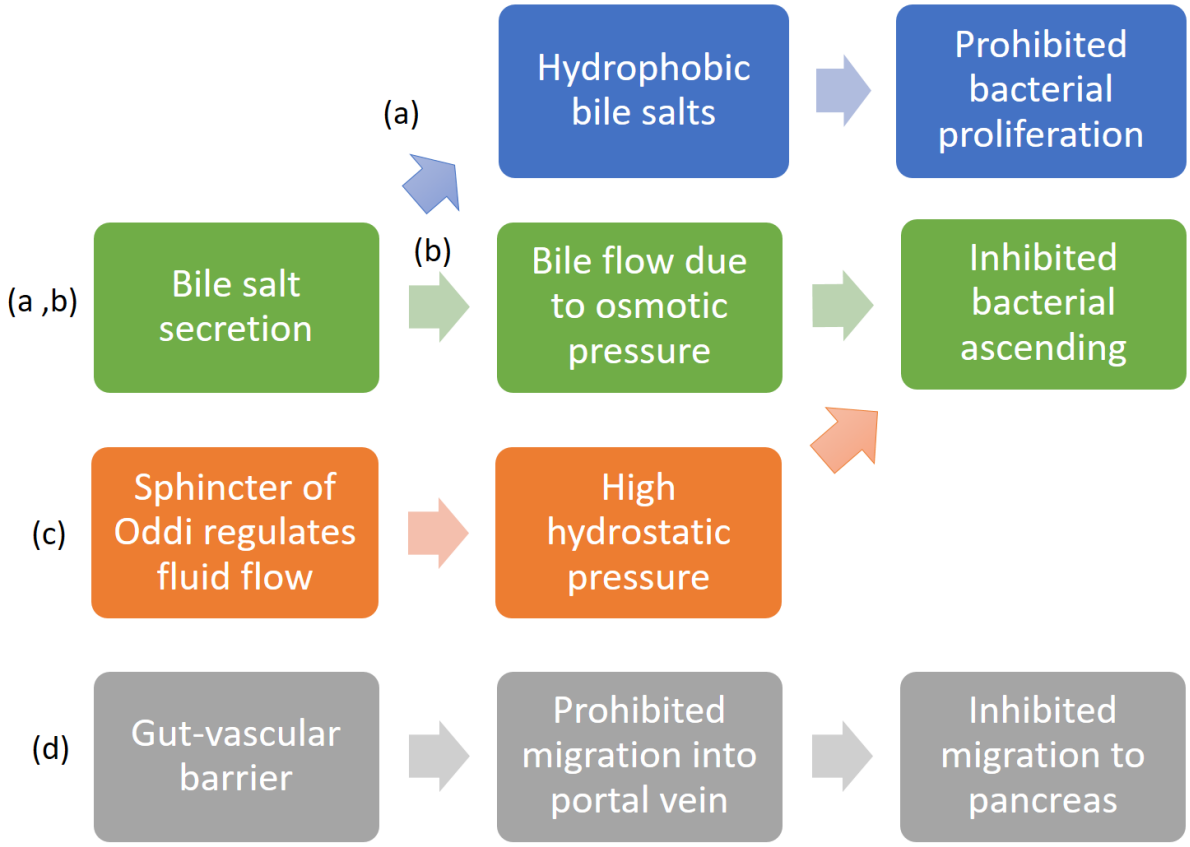

711

712 Figure 2. Defense mechanisms against bacterial invasion from the intestine into the pancreas(31,
713 77). Hydrophobic bile salts prohibit bacterial proliferation (a). Bile and pancreatic juice flow
714 prohibits bacterial invasion (**a**). The sphincter of Oddi, a muscle situated at the junction of the
715 biliary tract and duodenum, controls the flow of bile and pancreatic juice; the high-pressure zone
716 here prevents reflux of bacteria in the duodenum into the biliary tract(31) (**c**). The gut-vascular
717 barrier also controls the translocation of antigens and thus prevents the translocation of bacteria
718 from the gut through the portal vein to the liver or pancreas(77) (**d**).

719

720

721

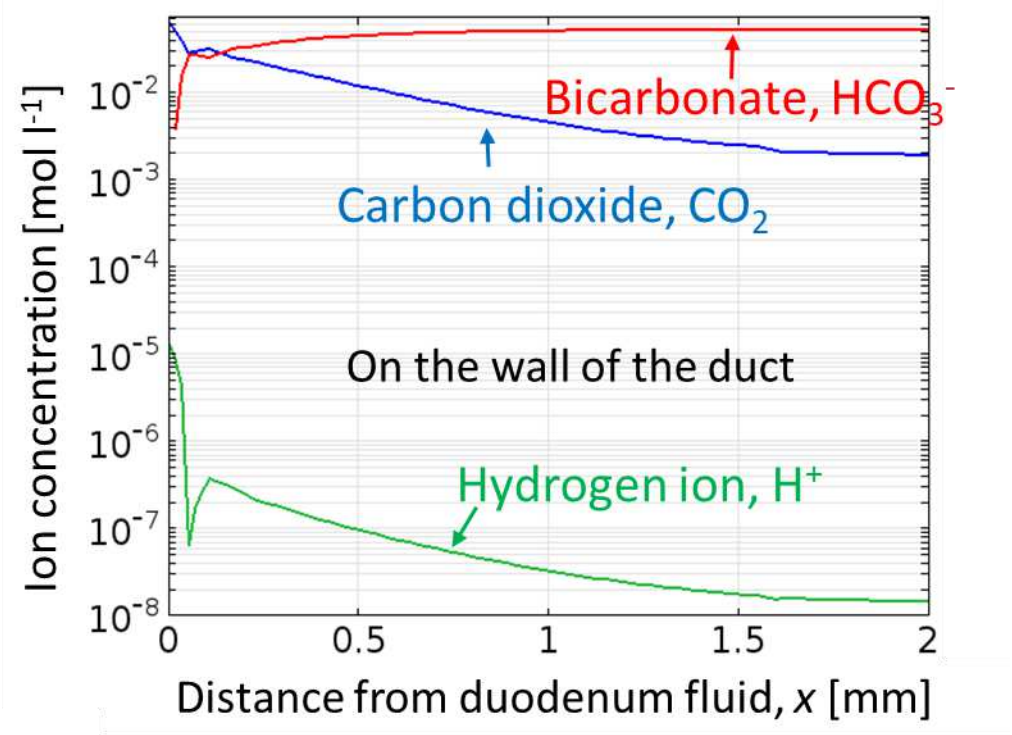

722

723 Figure 3. Simulated pH increased greatly between duodenal fluid and the pancreatic duct (**a**,
724 green), as hydrogen ions (**b** green) were neutralized by bicarbonate (**b** red) with carbon dioxide
725 as a byproduct (**b** blue). Simulated ion concentration distribution in the hepatopancreatic duct of
726 *healthy* individuals. Ion concentrations at a ductal radius of 4.1 mm (**b**)

727 $$pH = -\log_{10}([H^+])$$

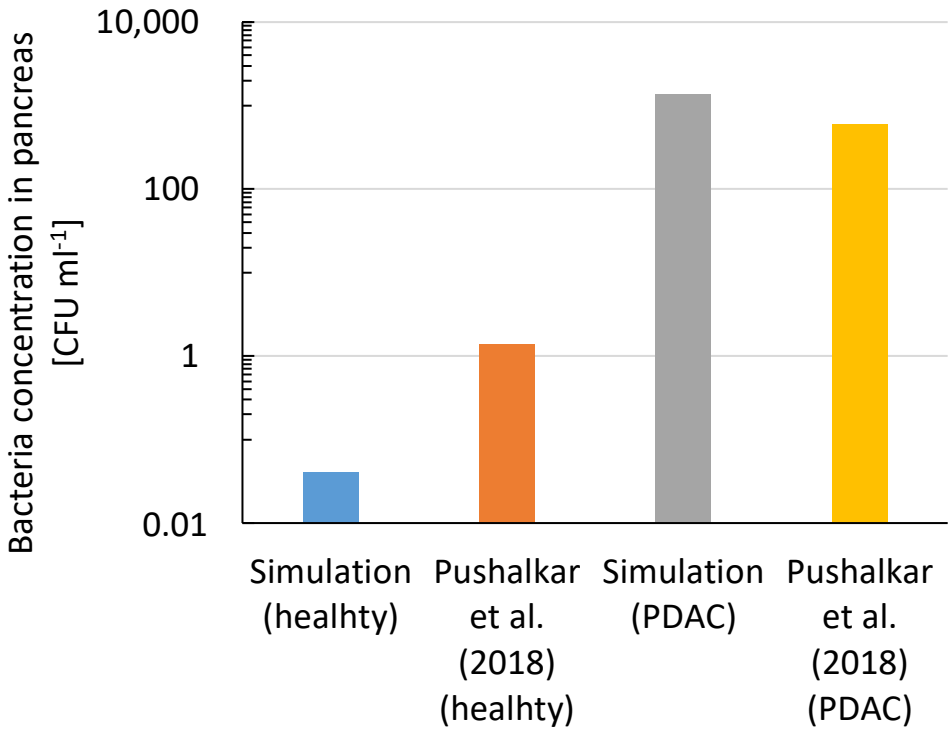

728

729 Figure 4. The simulated bacterial concentration in the healthy pancreas is lower than that in the
730 literature (blue), but that in the pancreas with tumors (green) agrees reasonably well with the
731 literature(10) (green). The literature value was calculated using the DNA weight of *E. coli* at 17
732 fg/cell(2). PDAC: pancreatic ductal adenocarcinoma

733

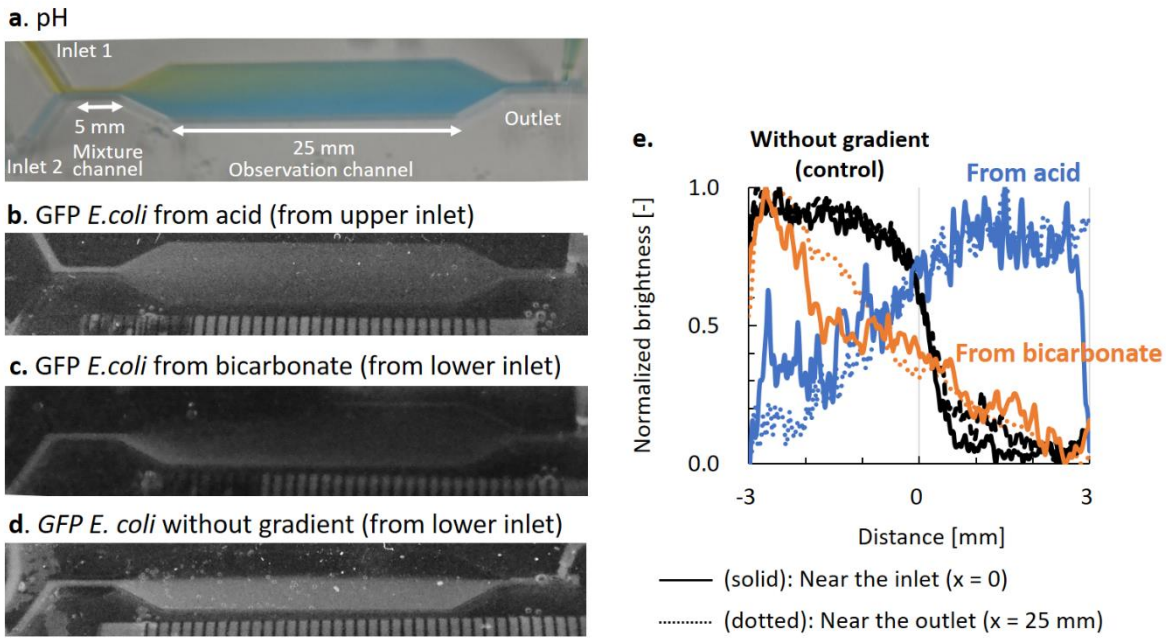

Figure 5. A steady pH gradient is generated in a microfluidic device, where the pH increases from 5–6 at the top to 7–8 at the bottom (**a**). GFP *E. coli* were attracted away from the upper channel with a lower pH toward the lower part with neutral pH due to pH taxis (**b**, **c, e** blue and orange). **a**: pH was visualized in bromothymol blue. **b**, **c**: Bacteria were included in either the upper inlet (**b**) or the lower inlet (**c**). **d**: GFP *E.coli* migrated little without gradient. **e:** Distribution of GFP *E. c*oli in the proximal (dotted) and distal (solid) channels. Photos in **b**–**d** were taken in black-and-white mode under black light at 350 nm.

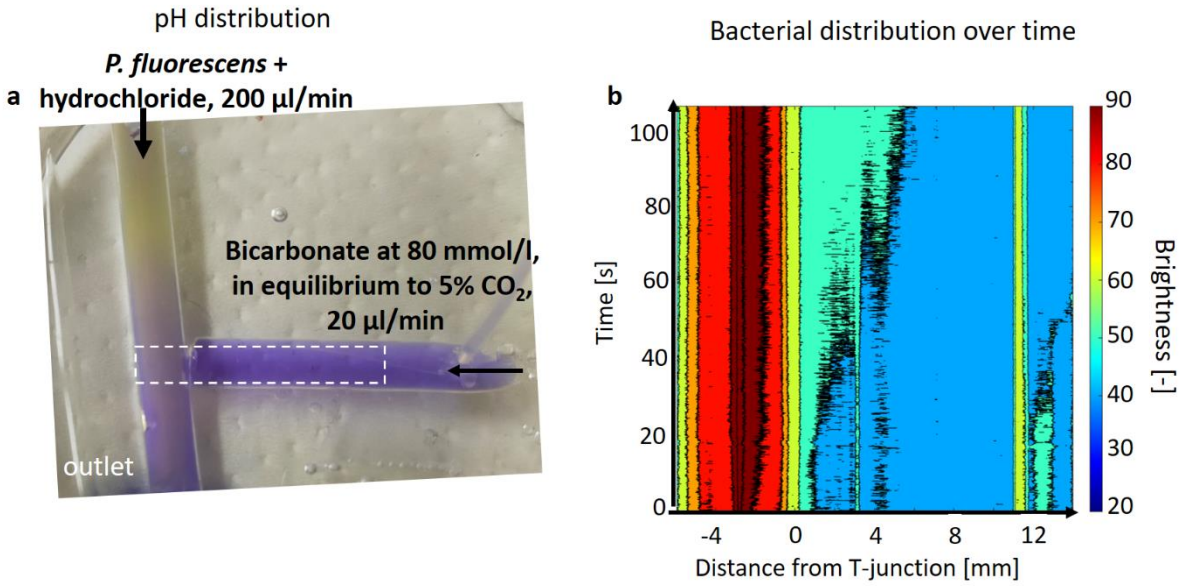

746

747 Figure 6. Measured upstream migrations of *P. fluorescens* against the flow of bicarbonate with a
748 maximum fluid velocity of 52 µm/s from hydrochloride solution in a simply fabricated PDMS T-
749 shaped cylinder. **a**: pH in the T-shaped cylinder, visualized in bromocresol purple. The pH
750 increased from 5–6 in dark yellow at top to neutral in purple at right. **b**: Bacterial distribution over
751 time in the white-dotted areas in **a**. *P. fluorescens* migrated upstream against flow under this pH
752 gradient (**a**) with a penetration rate of approximately 50 µm/s.

753

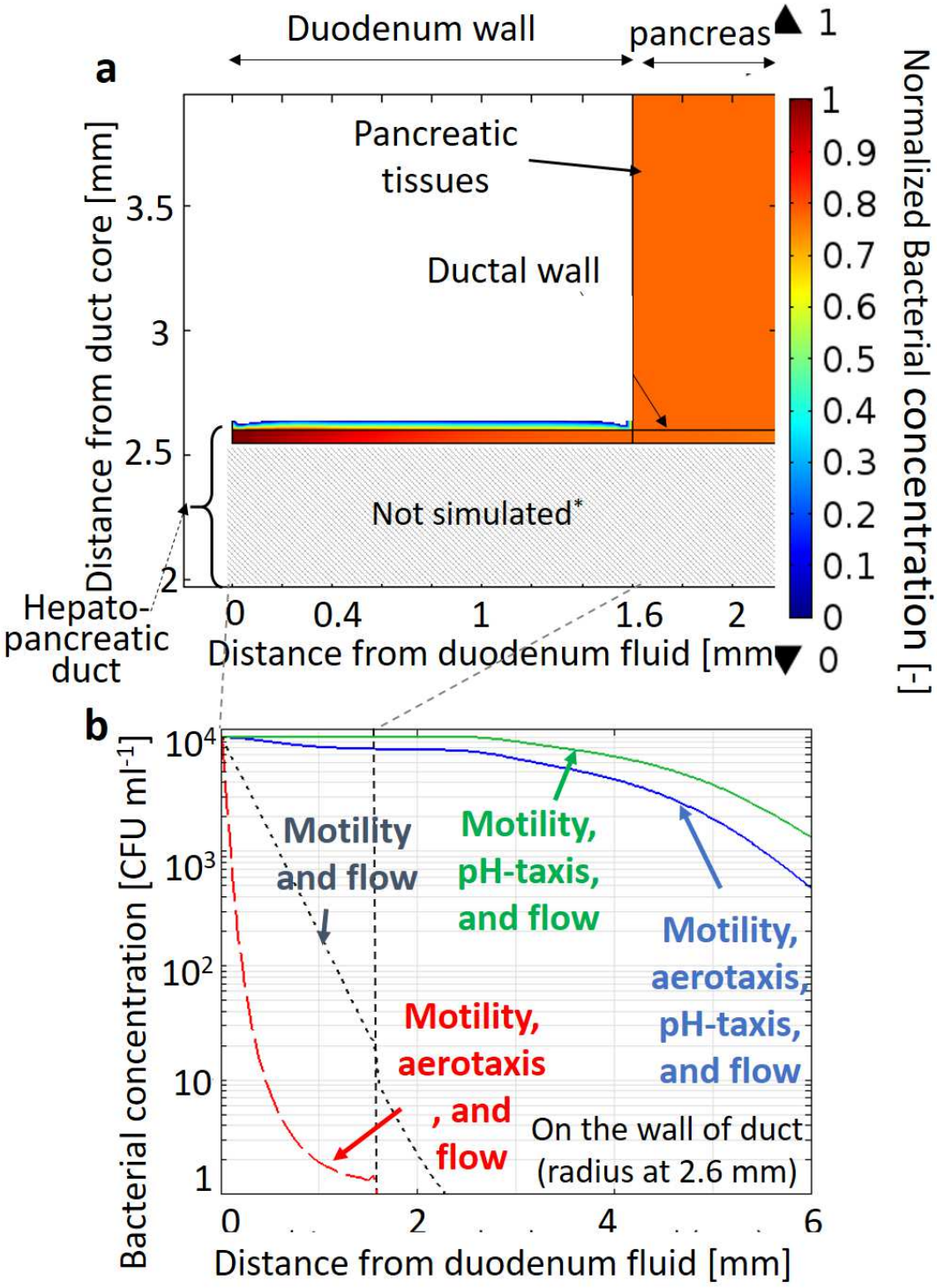

754

755 Figure 7. Migration of aerobic bacteria from the duodenum to the pancreas with tumors in the

hepatopancreatic duct is made easier by reduced pancreatic juice and bile flow rate due to obstructions of the pancreatic and bile duct by solid tumors

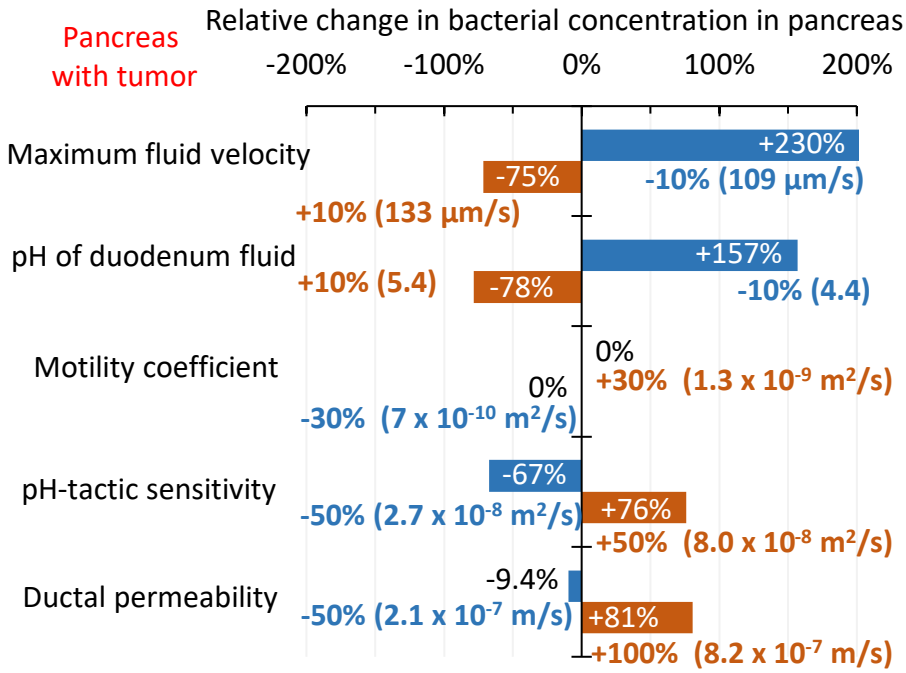

Figure 8. Parametric sensitivity analysis for bacterial migration from the duodenum into the pancreas with tumors.

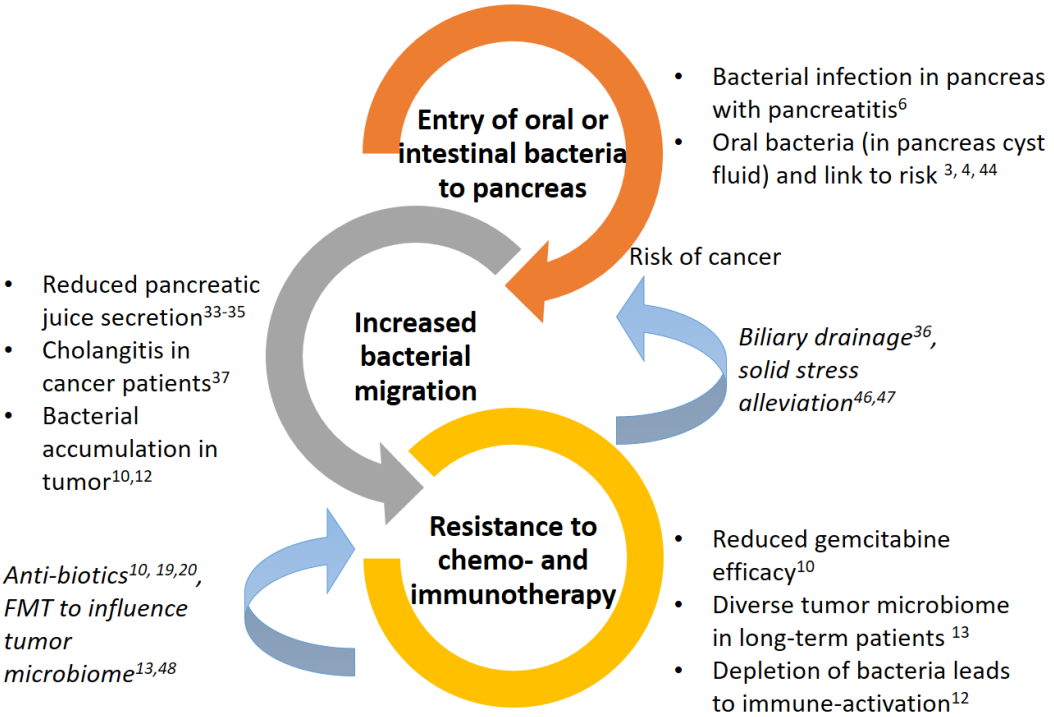

Figure 9. Hypothetical overview of involvement of oral or intestinal bacterial migration in risk, diseases, and resistance to treatment, with potential solutions.

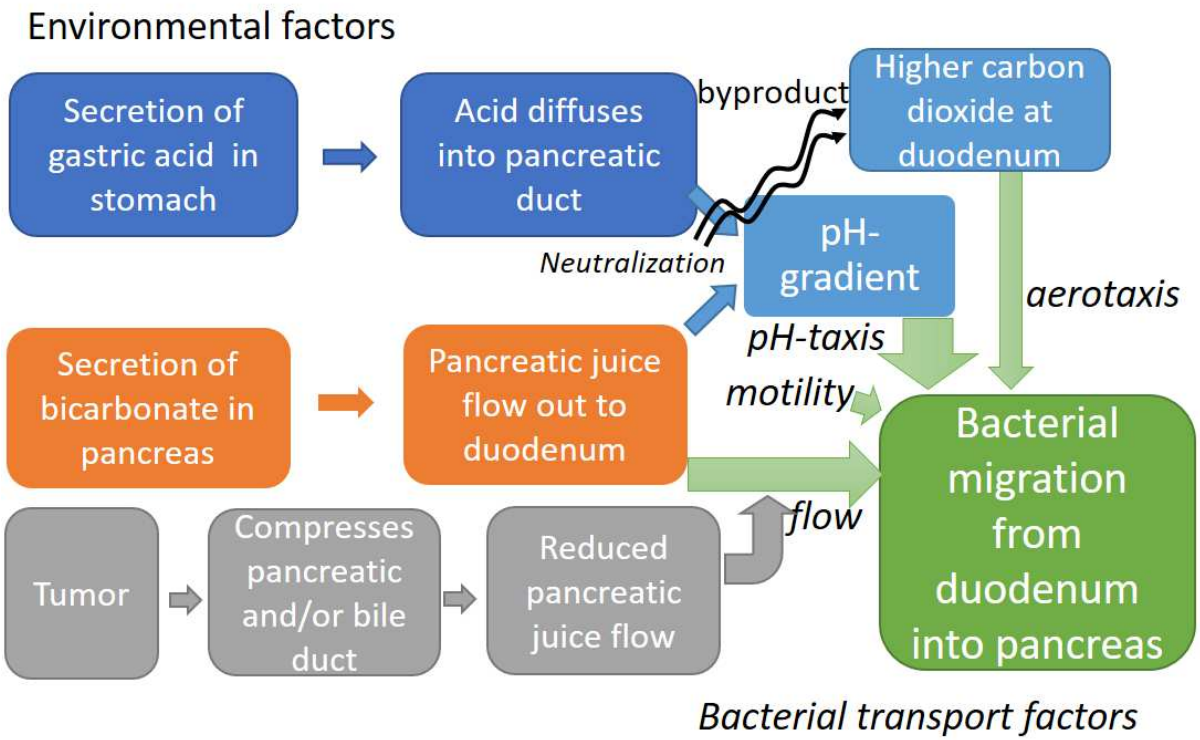

768

769 Figure 10. Environmental factors in the upper gastrointestinal tract affect the migration of aerobic

770 bacteria from the duodenum into the pancreas.

771

772

773

774 Table 1. List of the factors that influence transports included in this work

motility	Diffusion-like run-and-tumble random motion using flagellar, increases migration
chemotaxis	Migration toward chemoattractant or away from repellent
Aerotaxis	Energy taxis, toward higher oxygen (duodenum) (decreases migration) and away from higher carbon dioxide (duodenum) (increases migration) (for aerobes)
pH-taxis	Migration from acid or alkaline pH toward neutral one, increases migration

775

776

Supplementary Files

This is a list of supplementary files associated with this preprint. Click to download.

- supplemental1001edited2.zip